Modeling the influence of benthic primary production on oxygen transport through the water–sediment interface

César Ordoñez [a], Alberto de la Fuente [a,*], Paula Díaz-Palma [b]

[a] *Departamento de Ingeniería Civil, Universidad de Chile, Chile*
[b] *Ministerio del Medio Ambiente, Chile*

ABSTRACT

The context of this study is salty lagoons a few centimeters deep that are found in the arid region of the Andes Mountains in South America. The trophic structure of these aquatic ecosystems is supported by microalgae and photosynthetic bacteria located in the upper part of the sediment, and wind is the primary driver of mass and momentum transport through the water–sediment interface (WSI). This study proposes and validates, based on laboratory experiments, a simple algebraic expression computing dissolved oxygen (DO) exchange through the WSI considering benthic primary production. The algebraic expression was derived by vertically integrating DO diffusion-reaction equation in sediments divided into two layers: the upper heterogeneous layer where photosynthesis occurs and the lower layer where DO is consumed by biochemical reactions. Experiments were conducted in a wind tunnel with a water tank of variable depth that was at the downwind end of the experimental facility. Fresh sediments were placed in the middle of the tank such that DO was both consumed and produced in the sediments. This particular setup provides the required experimental conditions to measure the diffusion flux through the WSI, as well as the rate of consumption and production in the sediment, based on DO microprofiles. Based on 48 samples, the theoretical expression to compute the DO flux through the WSI was successfully validated. This expression can be used for computing DO exchanges fluxes across the WSI in shallow water bodies, where benthic primary production releases DO to the water during the day, and DO is consumed during the night.

© 2015 Elsevier B.V. All rights reserved.

1. Introduction

The central depressions of closed basins in the elevated plateaus of Chile, Argentina, Perú and Bolivia are characterized by landscapes formed by a crust of salt resulting from the evaporation of water in saline lakes (Risacher et al., 2003; de la Fuente and Niño, 2010; de la Fuente, 2014). These ecosystems, locally known salares, contain small and extremely shallow lagoons of a few centimeters deep, which are formed by inflows of groundwater that upwell at the perimeter of the salares and completely evaporate (Kampf et al., 2005; de la Fuente and Niño, 2010). Benthic communities develop in the upper part of the sediment in these lagoons (Hulbert and Chang, 1983; Demergasso et al., 2003). The dominant groups of benthic species are phototrophic bacteria and benthic microalgae, which produce oxygen, contributing to the stability of the sediments (Demergasso et al., 2003; Díaz-Palma et al., 2012)

and forming the basis for the higher tropic layers, such as aquatic macro-invertebrates and vertebrates (Hulbert and Chang, 1983; Dejoux, 1993; Mascitti and Kravetz, 2002).

One of the most important parameters that describe the dynamics of ecosystems is dissolved oxygen (DO; Wetzel, 2001). In shallow water columns, production and consumption of DO can be ignored. Consequently, the DO concentration in the water column is determined by the diffusive exchange through the air–water and water–sediment interfaces (Jørgensen and Des Marais, 1990; Dade, 1993; Guatieri and Gualtieri, 2008). Both DO fluxes are promoted by turbulence in the water column (Dade, 1993; Guatieri and Gualtieri, 2008). However, the DO flux through the water–sediment interface (WSI) also depends on diffusive transport within the sediments and the rate at which biochemical processes consume and produce DO (Boudreau and Jørgensen, 2001).

Previous studies of DO flux across the WSI focused only on sediment oxygen demand driven by biochemical consumption of DO in the sediment. This DO flux explains the generation of anoxic conditions in water lagoons, with the corresponding changes in chemical balances and water quality (Wetzel, 2001). By including benthic

* Corresponding author. Tel.: +56 2 29784401; fax: +56 2 2689 4171.
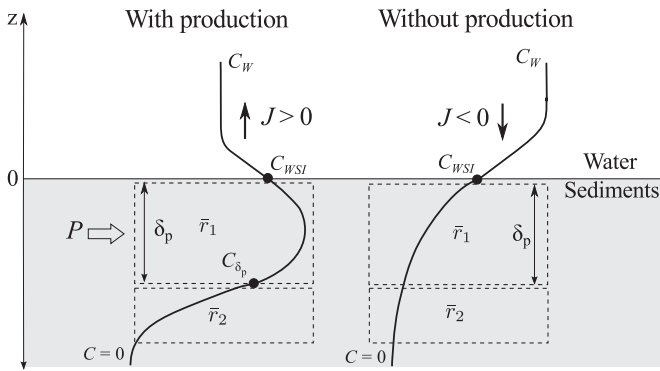 *E-mail address:* aldelafu@ing.uchile.cl (A. de la Fuente).

Fig. 1. Conceptual model for calculating DO exchanges across the WSI with (left) and without (right) primary production.

primary production, de la Fuente (2014) showed that the DO flux across the WSI (hereinafter called J) can be positive (toward the water column) or negative (toward the sediments) depending on the rates of DO production and consumption in the sediments and the DO concentration in the water column. However, de la Fuente (2014) considered homogeneous conditions in the sediments, and this assumption requires further analysis and validation. On the other hand, complex models for computing the DO flux across the WSI as a function of biochemical processes in the sediments have been developed (Boudreau, 1996; Cerco and Seitzinger, 1997; Sohma et al., 2008). However, these models either do not consider the turbulent transport in the water column, or are computationally expensive approaches that solve the diffusion-reaction equation of a large number of chemical compounds. Considering that in some practical applications, the use of complex models for the sediments impose computational restrictions, the main goal of this article is to propose a vertically integrated model for computing J, which takes into account processes that occur both in the water and on the sediment side and where the sediment side is characterized by vertical heterogeneity. The conceptual model divides the sediments into two layers: the upper heterogeneous layer where photosynthesis occurs and the lower layer where DO is consumed by biochemical reactions. This model allows us to perform modeling of exchange of DO across WSI for shallow lagoons. We then validate this model with experiments performed in a wind tunnel with a water tank of variable depth containing natural sediments with a thin layer of microalgae that produce DO.

2. Methods

2.1. Conceptual model

The conceptual model for studying DO exchanges through the WSI is shown in Fig. 1. From the water-side perspective, DO exchanges between sediment and water are caused by diffusive fluxes through the WSI, which can be computed as follows:

$$J = -D \frac{\partial C}{\partial z}\Big|_{z=0^+} = -k\left(C_W - C_{WSI}\right) \tag{1}$$

where D denotes the molecular diffusion coefficient that depends on the water temperature, C_W is the DO concentration in the bulk fluid, C_{WSI} is the DO concentration at the WSI, and k is the diffusional mass transfer coefficient. $J > 0$ implies that DO diffuses from the sediment to the water and vice versa (Fig. 1). From the sediment-side of WSI, DO flux can be modeled by solving the diffusion equation in the sediment. At steady state, the relationship can be calculated as

$$\phi D_s \frac{\partial^2 C}{\partial z^2} = r(z) - p(z) \tag{2}$$

where ϕ denotes the upper layer sediment porosity, D_s denotes the molecular diffusion coefficient modified by tortuosity effects and $p(z)$ and $r(z)(\mathrm{g\,r\,O_2\,m^{-3}\,d^{-1}})$ denote the volumetric rate of production and consumption of DO due to primary production and biochemical consumption, respectively (Revsbech et al., 1981; Kühl and Jørgensen, 1992; Bryant et al., 2010).

To include benthic primary production in the analysis, one must consider that this production occurs in a thin layer in the upper part of the sediment (Revsbech et al., 1986; MacIntyre et al., 1996; Cerco and Seitzinger, 1997). The depth of this layer is limited by the microalgae's need for light to perform photosynthesis. On the other hand three processes associated with DO consumption occur within the sediments: the respiration by photosynthetic microorganisms, the respiration by bacteria and oxygen uptake due to inorganic chemical reactions (Wetzel, 2001). As production and consumption due to photosynthetic organisms occur only within a layer of thickness δ_p, two uptake rates are considered in the model: one called $\bar{r}_1$, which is associated with the three processes of consumption (within δ_p), and another called $\bar{r}_2$, which represents the rate of consumption due to bacterial respiration and inorganic reactions below the photosynthetic active layer. According to previous results from Kühl and Jørgensen (1992), Rasmussen and Jørgensen (1992) and de la Fuente (2014), $\bar{r}_1$ and $\bar{r}_2$ are considered homogeneous.

Given mass conservation in the steady state, the vertically integrated rate of DO production should be

$$P = \bar{r}_1 \, \delta_p + J + \sqrt{2\phi D_s \, \bar{r}_2 \, C_{\delta_p}} \tag{3}$$

where the first term on the right-hand side of Eq. (3) denotes the rate of DO consumption within the active layer, J is the DO flux that diffuses toward the water column, and the last term represents the DO flux to the sediment below the photosynthetic active layer where it is consumed. Finally, C_{δ_p} is the concentration at $z = -\delta_p$.

The variability of the DO production rate in the sediment was taken into consideration in solving Eq. (2) for the active layer. This variability is due to the effect of light extinction through the sediment and the way microalgal metabolic processes react to different light intensities (Jørgensen and Des Marais, 1988; MacIntyre and Cullen, 1995; MacIntyre et al., 1996). To address this vertical variability, is important to introduce the coefficient α such that

$$\int_{-\delta_p}^{0} \int_{z}^{0} p\left(z'\right) dz' dz \approx \alpha \frac{\bar{p}\delta_p^2}{2} \tag{4}$$

where α accounts for the variability of the rate of DO production and $\bar{p}\delta_p = \int_{-\delta_p}^{0} p(z) \, dz$. In order to study the values of α we would consider simple distributions of $p(z)$ detailed in Table 1 and Fig. 2. All of the cases shown in Table 1 and Fig. 2 satisfy $p(-\delta_p) = 0$, and $p(z = 0)$ is the reference value called p_m. It is observed the case $\alpha = 1$ represents the case with homogeneous primary production in the active layer. A linearly distributed primary production is associated to $\alpha = 4/3$. Also, the case with the exponential decay of $p(z)$ characterized by a coefficient $k_p \, (m^{-1})$ provides $4/3 < \alpha < 2$, being the limit $\alpha = 2$ related to large values of k_p (see curve $\beta = k_p\delta_p = 50$ in Fig. 2). For convex distribution of $p(z)$, $1 < \alpha < 4/3$ was obtained. Given this, it is concluded that the parameter α takes values in between 1 and 2.

With the definition of α of Eq. (4), Eq. (2) was integrated twice to obtain C_{δ_p}. Further details of this double integration are given in Appendix.

$$C_{\delta_p} = -\frac{\left(\alpha P - \bar{r}_1 \delta_p\right)}{2\phi D_s} \delta_p + \frac{J}{\phi D_s} \delta_p + C_{WSI} \tag{5}$$

Table 1
Summary of calculus of shape factor α for different distribution of $p(z)$. p_m is the reference primary production at the WSI. Vertical profiles of $p(z)/p_m$ are shown in Fig. 2.

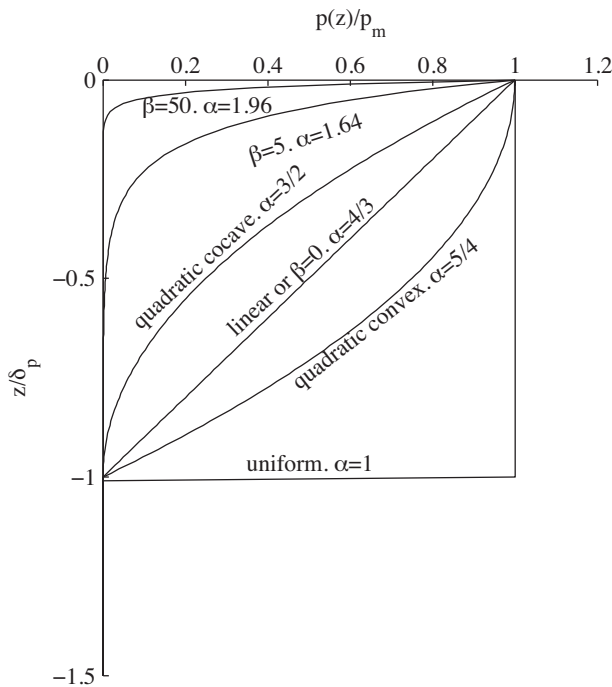|	$p(z)/p_m$	$\bar{p}/p_m$	$\frac{1}{\delta_p^2} \int_{-\delta_p}^{0} \int_{z}^{0} \frac{p(z')}{p_m} dz' dz$	α
Constant	1	1	$\frac{1}{2}$	1
Linear	$\left(1 + \frac{z}{\delta_p}\right)$	$\frac{1}{2}$	$\frac{1}{3}$	$\frac{4}{3}$
Quadratic concave	$\left(1 + \frac{z}{\delta_p}\right)^2$	$\frac{1}{3}$	$\frac{1}{4}$	$\frac{3}{2}$
Quadratic convex	$\left(1 - \left(\frac{z}{\delta_p}\right)^2\right)$	$\frac{2}{3}$	$\frac{5}{12}$	$\frac{5}{4}$
Exponential decay ($\beta = k_p \delta_p \geq 0$)	$\dfrac{\left(e^{k_p z} - e^{-\beta}\right)}{\left(1 - e^{-\beta}\right)}$	$\dfrac{\left(e^{-\beta}(1+\beta) - 1\right)}{\left(1 - e^{-\beta}\right)\beta}$	$\dfrac{\left(e^{-\beta}\left(\frac{\beta^2}{2} - 1\right) + 1 - \beta\right)}{\left(1 - e^{-\beta}\right)\beta^2}$	$\frac{4}{3}$; $\quad \beta \to 0$ 2; $\quad \beta \to +\infty$ 1.64; $\quad \beta = 5$

Fig. 2. Simple vertical distribution of primary production used for estimating the parameter α in Table 1.

Eq. (5) is multiplied by $S_2 = 2\phi D_s \bar{r}_2$, and the obtained equation is combined with Eq. (3) to obtain

$$C_{WSI} S_2 = (P - J)^2 - P(P - P_{ef}) + \Delta \bar{r} \delta_p (2J - P_{ef}) - (1 - \alpha) \bar{r}_2 \delta_p P \tag{6}$$

where $\Delta \bar{r} = \bar{r}_1 - \bar{r}_2$, $P = \bar{p}\delta_p$ and $P_{ef} = P - \bar{r}_1 \delta_p$, which defines the effective rate of DO production, corresponding to the DO that is not locally consumed in the active layer. In other words, P_{ef} is the DO that is free to diffuse toward the atmosphere or deeper sediments where it is finally consumed at a rate $\bar{r}_2$. In the case of $P_{ef} > 0$, Eq. (6) is inserted into Eq. (1) to obtain a second order polynomial equation whose solution is given by

$$J = \frac{S_2}{2}\left[\left(\frac{1}{k} + 2\frac{P_a}{S_2}\right)\right.$$
$$\left. - \sqrt{\left(\frac{1}{k} + 2\frac{P_a}{S_2}\right)^2 - 4\left(\frac{P_a P_{ef}}{S_2^2} - \frac{C_W}{S_2} - (1-\alpha)\frac{\bar{r}_2 \delta_p P}{S_2^2}\right)}\right] \tag{7}$$

where $P_a = P - \Delta \bar{r} \delta_p$. The detailed derivation of this step is given in Appendix. If, however, $P_{ef} < 0$, two cases are possible: one where the DO is consumed within the active layer, and the second where DO

is consumed in a thicker region of the sediments than δ_p. In both cases, the effective rate of DO consumption in the active layer is defined as $\bar{r}_3 = \bar{r}_1 - \alpha P/\delta_p$. With this definition, the first case occurs if $J/\bar{r}_3 < \delta_p$, where J is calculated as follows

$$J = \frac{S_3}{2}\left[\left(\frac{1}{k}\right) - \sqrt{\left(\frac{1}{k}\right)^2 - 4\frac{C_W}{S_2}}\right] \tag{8}$$

with $S_3 = 2\phi \bar{r}_3 D_s$. The case described by Eq. (8) is equivalent to the DO consumption in homogeneous sediment first derived by Nakamura and Stefan (1994). In the second case, where DO is consumed in a thicker region of the sediments than $J/\bar{r}_3 > \delta_p$, J is calculated as follows

$$J = \frac{S_2}{2}\left[\left(\frac{1}{k} + 2\frac{2\Delta \bar{r}_2 \delta_p}{S_2}\right)\right.$$
$$\left. - \sqrt{\left(\frac{1}{k} + 2\frac{2\Delta \bar{r}_2 \delta_p}{S_2}\right)^2 + 4\left(\frac{2\Delta \bar{r}_2 \delta_p}{S_2^2} + \frac{C_W}{S_2}\right)}\right] \tag{9}$$

where $\Delta \bar{r}_2 = \bar{r}_3 - \bar{r}_2$. The algorithm for computing J as a function of the parameters of the problem ($\bar{r}_1, \bar{r}_2, P, \alpha, C_W, \phi, D_s$ and k) requires determining whether $P_{ef} = P - \bar{r}_1 \delta_p$ is positive or negative. If $P_{ef} \geq 0$, Eq. (7) is used to calculate J. Otherwise ($P_{ef} < 0$), J should first be estimated using Eq. (8). If $J/\bar{r}_3 < \delta_p$, Eq. (8) is representative of the problem; otherwise Eq. (9) should be used to determine J.

2.2. Experimental procedure

Experiments were performed in the Francisco Javier Dominguez Hydraulics Laboratory of Universidad de Chile, in a wind tunnel with a 4 m long, 0.5 m wide, and 0.5 m deep tank, at the downwind end (Fig. 3). The tank contains a variable depth false bottom with open ends at each side, both upwind and downwind, so the wind-dragged water is allowed to recirculate below the false bottom. The water depth above the false bottom, h, was 3 or 5 cm. Moreover, in the middle of the false bottom, a 0.15 m long compartment was filled with fresh sediments (Fig. 3) with a thin layer of microalgae that produce DO, collected from the artificial lagoon O'Higgins Park near the university campus in Santiago, Chile.

The microalgae layer in the top layer of the sediments was developed by filling the tank with a nutrient solution obtained from a mix of drinking water (90%) and natural water from the same lagoon as the sediments. The tank was kept agitated by running the wind tunnel 9 h per day, and cold white LED lights were installed over the tank, exposing the surface of the sediment to 2950 lx with a photoperiod of 16 h of light and 8 h of dark. Additionally, eight 300 W heaters were used to control the water temperature in the range of 24–25 °C. This basic configuration was maintained for approximately two months, during which the evaporated water
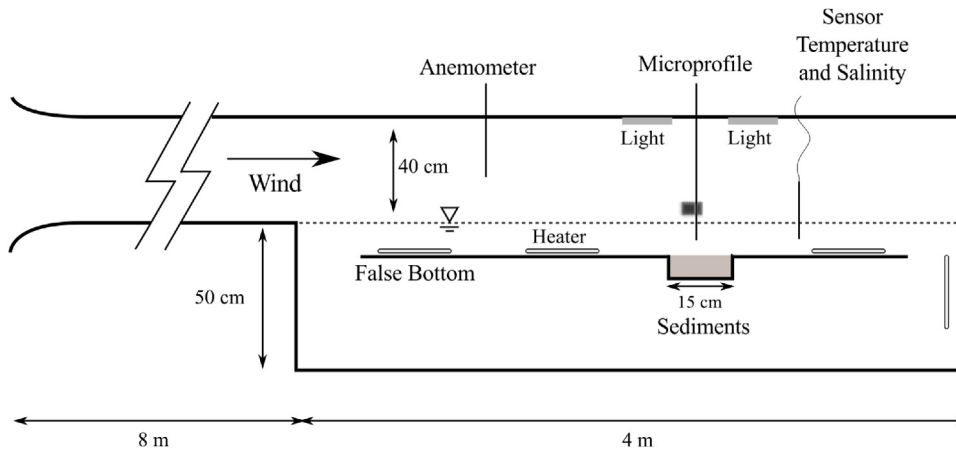
Fig. 3. Experimental setup.

was replaced with the same mix of 90% of drinking water and 10% of natural water from the lagoon. Following this growth period, all the experiments were conducted over approximately two weeks, thus ensuring similar physiological conditions of the microalgal community.

Each experiment was characterized by the water depth h above the false bottom, and the wind shear velocity, u_*. Both h and u_* define k_t (Arega and Lee, 2005; Nakamura and Stefan, 1994; O'Connor and Hondzo, 2008; Steinberger and Hondzo, 1999). The water depth varied between 3 and 5 cm while the four wind shear velocities used were between 0 (no wind) and 2.27 cm s^{-1}. For each experiment, the following measurements were conducted: (i) vertical profiles of wind speed were measured with an Extech hot-wire anemometer. Each wind velocity profile was constructed with measurements spaced every 1 cm the first two centimeter at the water surface and 2 cm above that distance. At each elevation, the anemometer sampling rate was set to 0.2 Hz, and the wind velocity was determined by averaging 30 s of measurements. (ii) At the downwind end of the sediment compartment, DO micro-profiles at both sides of the WSI were measured with an OX-25 Unisense microprobe with an outer tip of 25 μm. The microprobe was connected to a Microsensor Multimeter Unisense signal amplifier. The vertical spacing between two consecutive points of the DO micro-profiles was set to 160 μm; this fine vertical displacement was achieved by a semi-automatic motor that moves the sensor with a resolution of 80 μm. The sampling rate for the DO microelectrode was 1 Hz, and the DO concentration used for the micro-profile was the temporal average of 60 s of measurements. For each experimental combination of h and u_*, conditions with and without benthic primary production were characterized with six micro-profiles, three for conditions with primary production, and three for conditions without light. Turning the lights on or off was used to regulate primary production. The methodology for processing micro-profiles is detailed in the following section. (iii) Finally, water temperature and salinity were measured with a TetraCon 925 conductivity and temperature sensor connected to data Multi 340i data logger.

Finally, in order to describe the upper part of the sediment (5–6 mm), a Kimax-51 capillary glass with a 1 mm inner diameter was mounted to the semi-automatic motor to sample the vertical structure of the sediments. The contents of the capillary were analyzed with a 2× magnifying lens to determine the thickness of the microalgae layer (δ_p). To further describe this photosynthetic active layer, thin slices of sediment were removed from the capillary and observed on a microscope to identify groups of dominant benthic species.

2.3. Data processing: DO micro-profiles

DO micro-profiles were processed to determine the parameters required in Eqs. (7)–(9) (see also Fig. 1). The particular parameters of interest were the thickness of the photosynthetic active layer (δ_p), the rates of DO consumption in and below δ_p ($\bar{r}_1$ and $\bar{r}_2$, respectively, both of which were considered homogeneous in the corresponding regions), vertical profiles of $p(z)$, J and the sediment porosity ϕ. DO micro-profiles were analyzed taking into account processes on both sides of the WSI.

First, when $p(z) = 0$ and $\bar{r}_1$ and $\bar{r}_2$ are constant, Eq. (2) reduces to a parabolic function. With this information, micro-profiles without light were used to measure $\bar{r}_1$ by fitting a quadratic function to the entire set of measurements between the WSI and δ_p. Then, to obtain the vertical profile of $p(z)$, Eq. (2) was integrated over the control volume of the ith point in the micro-profile. Here $i = 1$ corresponds to the surface. The thickness of the control volume is $\Delta z = z_{i-1} - z_{i+1}$. In this way, Eq. (2) integrated over the control volume was written as

$$\int_{z_{i+1}}^{z_{i-1}} (\bar{r}_1 - p(z)) \, dz \approx (\bar{r}_1 - p_i) \, \Delta z = \phi D_s \left(\left. \frac{\partial C}{\partial z} \right|_{z_{i-1}} - \left. \frac{\partial C}{\partial z} \right|_{z_{i+1}} \right) \tag{10}$$

where p_i denotes the volumetric rate of DO production of the ith point of the micro-profile, and the vertical gradients of C evaluated at z_{i-1} and z_{i+1} were estimated with a linear fit of the DO concentration using measurements $i-2$, $i-1$ and i for $\partial C/\partial z|_{z_{i-1}}$ and i, $i+1$ and i, $i+2$ for $\partial C/\partial z|_{z_{i+1}}$. Therefore,

$$p_i = \frac{\phi D_s}{z_{i-1} - z_{i+1}} (B_{i+1} - B_{i-1}) + \bar{r}_1 \tag{11}$$

where B_{i+1} and B_{i-1} are the slopes of the linear fit required for the vertical gradient of C at $z = z_{i+1}$ and z_{i-1}, respectively. With this information, the elevation of the WSI (z_{WSI}) was determined by identifying the elevation where B_i was at its maximum and $p_i - \bar{r}_1$ was zero. Under light conditions, the photosynthetic zone (δ_p) was manually defined as the depth below the WSI where $p_i > 0$. Once δ_p was defined, $\bar{r}_2$ was obtained by fitting a parabolic function to measurements below δ_p in micro-profiles with primary production. An alternative computational method, described by Revsbech et al. (1981), was used to process micro-profiles with $h = 3$ cm wind shear velocity of $u_* = 0.30$, 0.54, and 0.65 m s^{-1}. This method calculated the rates of production based on the temporal change of DO concentration, in contrast, the method that we propose, uses the spatial changes to calculate the rates of production.

With respect to the measurement of J, the DO concentration at the WSI was obtained by evaluating $C_{WSI} = B_{WSI} z_{WSI} + A_{WSI}$, where B_{WSI} and B_{WSI} are the coefficients of the linear fit for the points that define the WSI. Combining Eq. (1) and the DO flux on the sediment side of the WSI ($i = WSI + 1$), the DO flux was calculated as

$$J = \frac{\phi D D_s}{\phi D_s + D}(B_{WSI} + B_{WSI+1}) \tag{12}$$

where D is the molecular diffusion coefficient in the water that depends on the measured water temperature, and ϕ is the porosity in the upper layer of the sediment. Additionally, following Bryant et al. (2010), $D_s \approx \phi D$. With this approximation, flux continuity at the WSI allowed us to write:

$$\phi^2 \left.\frac{\partial C}{\partial z}\right|_{z^-} = \left.\frac{\partial C}{\partial z}\right|_{z^+} \tag{13}$$

where $\partial C/\partial z|_{z^-}$ and $\partial C/\partial z|_{z^+}$ are B_{WSI+1} and B_{WSI+1}, respectively (Jørgensen and Boudreau, 2001). Then, the representative value of ϕ for the entire set of experiments was obtained by fitting a line ($y = Mx$) to the entire data set of $\partial C/\partial z|_{z^-}$ and $\partial C/\partial z|_{z^+}$.

This methodology is iterative in the sense that δ_p is defined by identifying the depth at which $p_i = 0$, for which it is required to know $\bar{r}_1$, which depends on δ_p.

3. Results

3.1. Qualitative description of the microbial mat

One of the objectives of the capillary glass was to measure the thickness of the upper layer where benthic microalgae grow and to compare this measurement with the value of δ_p estimated from the DO micro-profiles. Fig. 4 shows the upper part of sediments where a thin green layer is observed over the brown sediments. This upper layer was 1.1 mm thick. The microscope analysis of the green layer showed the presence of diatoms (*Amphora* sp., *Navícula* sp., and *Cymbella* sp.), filamentous cyanobacteria (*Lybia* sp., *Phormidium* sp. and *Plectonena* sp.), bacterial colonies and protozoa. A qualitative analysis with the microscope showed that the
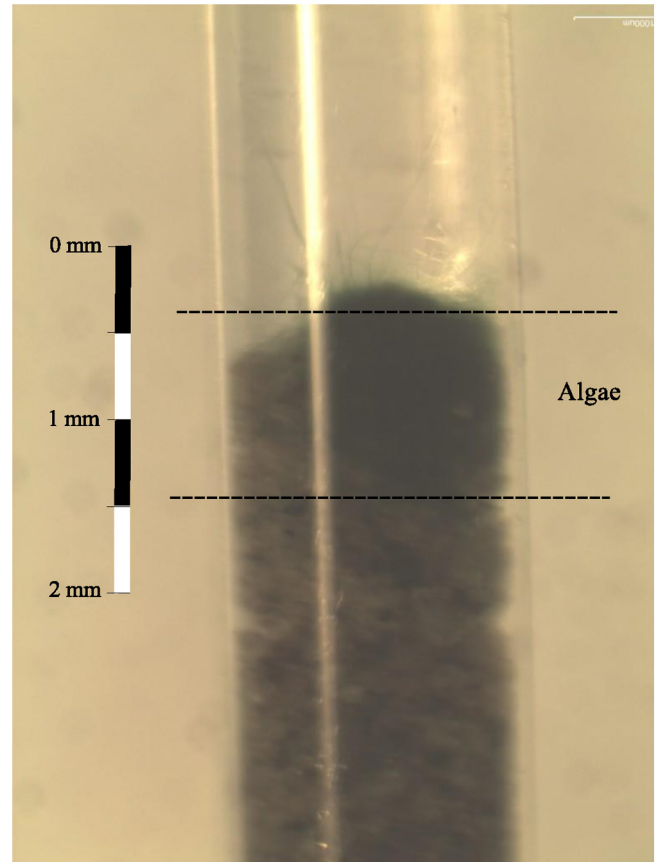

Fig. 4. Picture of a sediment sample obtained with a glass capillary.

abundance of microalgae decreased with the depth of the sediment. Together with organic matter mineralization, the respiration of these organisms defines the rate of DO consumption in the sediments.
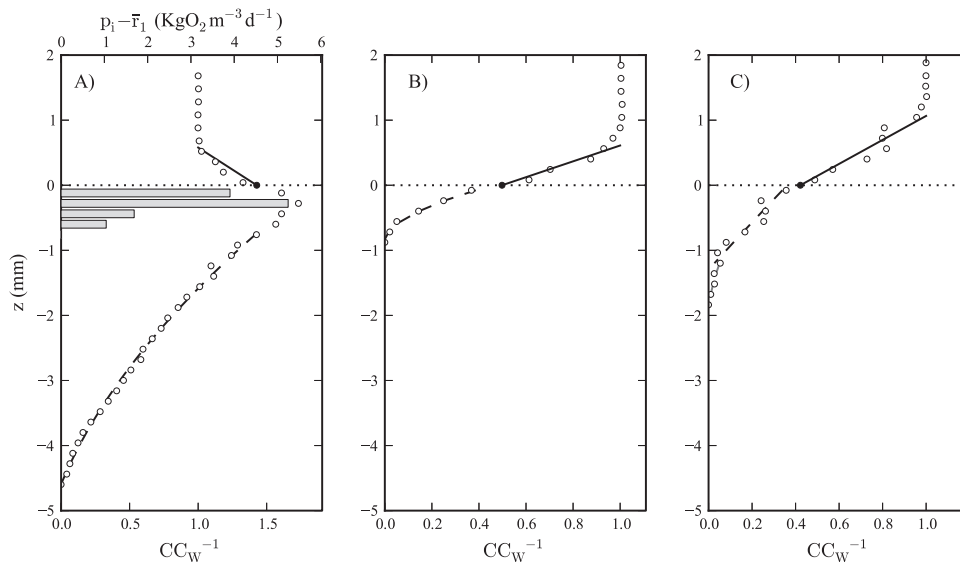

Fig. 5. (A) An example of a micro-profile that represents Eq. (7), with light, $h = 3$ cm, and $u_* = 1.15$ cm s^{-1}. Horizontal bars indicate measured rates of DO production (Eq. (11)), the solid line shows the linear fit used to measure J, and the dashed line shows the quadratic fit used to measure $\bar{r}_2$. (B) An example of a micro-profile without light where DO consumption only takes place within δ_p, represented by Eq. (8). This profile was generated without light, $h = 3$ cm, and $u_* = 0.87$ cm s^{-1}. The solid line shows the linear fit used to measure J, and the dashed line shows the quadratic fit used to measure $\bar{r}_1$. (C) An example of a micro-profile without light where DO consumption also takes place below δ_p, represented by Eq. (9). This profile was generated without light, $h = 3$ cm, and $u_* = 2.27$ cm s^{-1}. The solid line shows the linear fit used to measure J, and dashed line shows the quadratic fit used to measure $\bar{r}_1$.
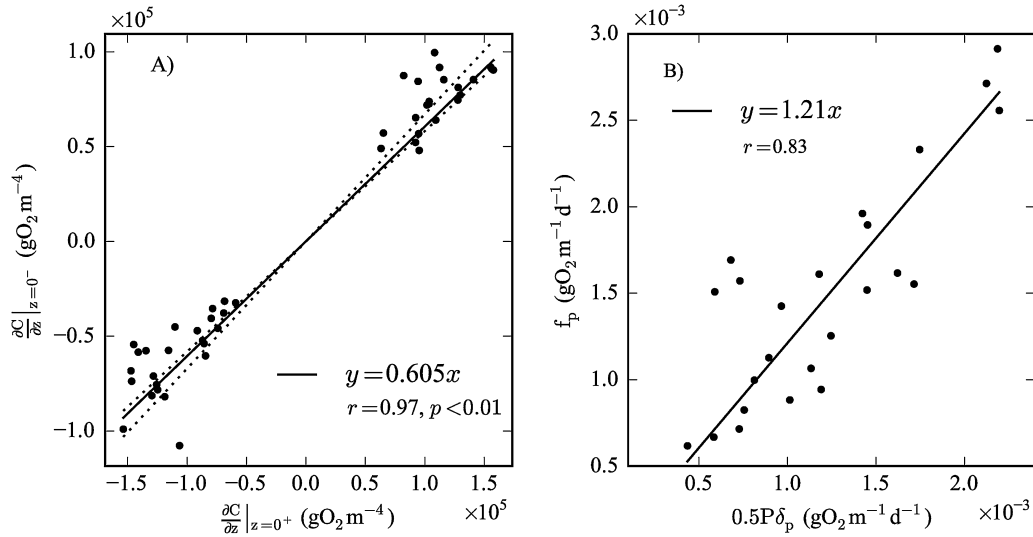
Fig. 6. (A) Estimation of the sediment porosity based on Eq. (13). (B) Estimation of the parameter α based on Eq. (4). $f_p = \int_{-\delta_p}^{0} \int_{z}^{0} p(z')dz'dz$.

3.2. Micro-profile processing

Fig. 5 shows the results obtained from processing three DO micro-profiles for conditions with light (Fig. 5A, Eq. (7)), without light when DO is consumed in the photosynthetic active layer (Fig. 5B, Eq. (8)), and without light when DO is also consumed below δ_p (Fig. 5C, Eq. (9)). Horizontal bars in Fig. 5A show the estimated primary production calculated using Eq. (11); the dashed line shows the fitted quadratic function used to obtain $\bar{r}_2$. Micro-profiles without light were used to measure $\bar{r}_1$, and Figs. 5B and C show the two different cases identified: Fig. 5B depicts the DO consumption described by Eq. (8), where DO is consumed in the photosynthetic active layer; Fig. 5C shows a characteristic micro-profile for the scenario described by Eq. (9), where DO is also consumed below δ_p. Additionally, sediment porosity ϕ was obtained using Eq. (13), as shown in Fig. 6A. The equation yielded $\phi^2 = 0.605 \pm 0.045$, which is equivalent to $\phi = 0.78$.
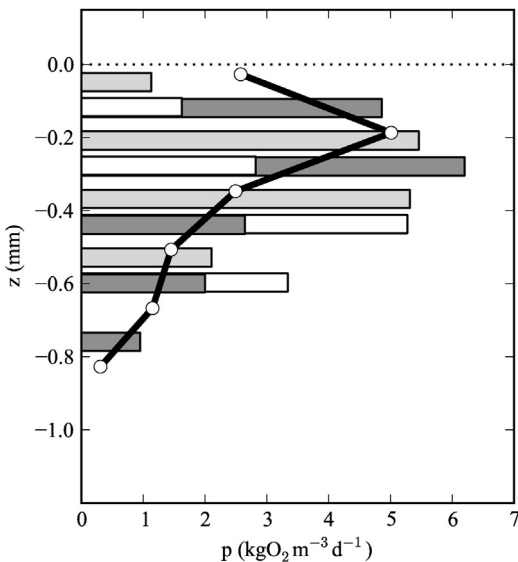

Fig. 7. Comparison of measured DO production rates ($p(z)$) from experiments with $h = 3$ cm and $u_* = 1.15$ cm s^{-1}. Horizontal bars indicate values of p measured with Eq. (11) for the three replicate micro-profiles, and the solid line shows values of p generated using the methods from Revsbech et al. (1981).

Once the entire set of micro-profiles was processed, the coefficient α defined in Eq. (4) was calculated by integrating $p(z)$ to obtain P and by integrating Eq. (4). Fig. 6B shows the value of the double integral of Eq. (4) which was integrate numerically and called f_p as a function of $0.5\bar{p}\delta_p^2$. The slope of the curve is the coefficient α. A constant value of $\alpha = 1.21 \pm 0.18$, which is in the expected order of $1 < \alpha < 2$ defined in Table 1 and Fig. 2, was obtained. Thus, the vertical profile of $p(z)$ influences the DO exchange at the WSI. This vertical variability is shown in Fig. 7, which compares $p(z)$ measured in the experiment $h = 3$ cm and $u_* = 1.15$ cm s^{-1} based on Eq. (11) (horizontal bars) and the Revsbech et al. (1981) methodology (white circles and solid line). Horizontal bars correspond to the range of results for three replicate micro-profiles measured for the experiment. Similarly to Jørgensen et al. (1983), Fig. 7 shows that the maximum rate of DO production occurs below the WSI (between 0.2 and 0.4 mm), and the decays to zero with distance. This general pattern was observed with both methodologies, although whether it is due to photo inhibition near the WSI or because the microalgae biomass is not uniform in the photosynthetic active layer (e.g., Hancke et al., 2014) is unclear. Additionally, both methodologies provide similar values of $p(z)$, which supports our methodology for processing the micro-profiles.

3.3. DO fluxes at the WSI

The average values for the set of micro-profiles are summarized in Table 2. The value of δ_p estimated with micro-profiles was 0.96 mm which is consistent with $\delta_p = 1.1$ mm observed in the capillary glass. Additionally, $\bar{r}_1$ was approximately one order of magnitude larger than $\bar{r}_2$, which indicates that DO is mostly recycled in the photosynthetic active layer. This statement is justified by looking at the effective DO production ($P_{ef} = P - \bar{r}_1\delta_p$), which was of the same order of magnitude as the net consumption

Table 2
Summary of measured parameters.

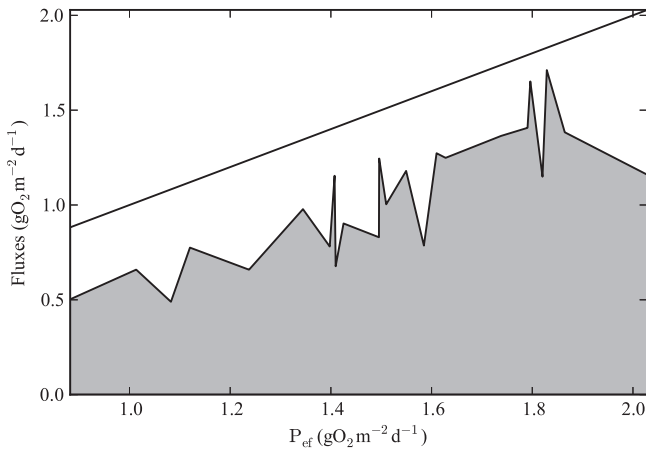| Parameter	Range
k (m d^{-1})	0.113–0.807
$\bar{r}_1$ (g O$_2$ m^{-3} d^{-1})	335–2543
$\bar{r}_2$ (g O$_2$ m^{-3} d^{-1})	40–323
δ_p (mm)	0.51–1.52
P_{ef} (g O$_2$ m^{-2} d^{-1})	0.882–2.028
C_{WSI} (g O$_2$ m^{-3})	1.53–14.28

Fig. 8. Partitioning of P_{ef} between J (gray area) and the rate of DO consumption below δ_p (white area below diagonal).

of DO in δ_p ($\bar{r}_1\delta_p = 0.92\,\mathrm{g\,O_2\,m^{-2}\,d^{-1}}$). Consequently, because $P_{ef} = 1.50\,\mathrm{g\,O_2\,m^{-2}\,d^{-1}}$, approximately the 40% of the DO produced is consumed by respiration and biochemical consumption within δ_p. With respect to the rate of P_{ef}, Eq. (3) shows that DO can either diffuse toward the atmosphere ($J > 0$) or be consumed below δ_p at a rate $\bar{r}_2$. Fig. 8 plots the partitioning between P_{ef} in terms of J (gray area) and consumption below δ_p as a function of P_{ef} (white area below diagonal line). Fig. 8 shows that the increase in P_{ef} is primarily reflected in the increase of J, rather than an increase in the DO flux toward the deeper sediments. For example, $J \approx 1.5\,\mathrm{g\,O_2\,m^{-2}\,d^{-1}}$ was observed for experiments with $P_{ef} = 2\,\mathrm{g\,O_2\,m^{-2}\,d^{-1}}$, while for $P_{ef} = 1\,\mathrm{g\,O_2\,m^{-2}\,d^{-1}}$, $J \approx 0.4\,\mathrm{g\,O_2\,m^{-2}\,d^{-1}}$. As a consequence, the DO flux toward deeper sediments was nearly constant and independent of P_{ef} ($P_{ef} - J \approx 0.52\,\mathrm{g\,O_2\,m^{-2}\,d^{-1}}$).

3.4. Validation of the conceptual model

The conceptual model for computing J described in Eqs. (7)–(9) was tested against observations, and the direct comparison between observed (J_o) and predicted (J_p) values of J is shown in Fig. 9. White circles were calculated with Eq. (7) and represent conditions where $P_{ef} > 0$ (Fig. 5A). Gray circles were calculated with Eq. (8) and represent cases where $P_{ef} < 0$ and DO is completely consumed in δ_p at a rate $\bar{r}_3 = \bar{r}_1 - \alpha P/\delta_p$ (Fig. 5B). Finally, black circles were calculated with Eq. (9) and represent the case where DO is also consumed below δ_p (Fig. 5C).

Fig. 9 shows that observed values of J were well predicted by Eq. (7)–(9), with a correlation coefficient $R = 0.98$, thus validating the conceptual model proposed in this article. To explore the behavior that predicts Eq. (7)–(9) as a function of the hydrodynamic conditions in the water column (k), Fig. 10 shows predicted values of the dimensionless $J/(S_1 C_W)^{1/2}$ and C_s as a function of $k_* = kC_W/(S_1 C_W)^{1/2}$. Here, $(S_1 C_W)^{1/2}$ is the maximum DO flux consumed in homogeneous sediment for the limit $k_* \to \infty$ (Nakamura and Stefan, 1994; de la Fuente, 2014). For any value of P, $|J|$ rapidly increases with k_* (Fig. 10A), which demonstrates that J can be limited by turbulence in the water column. In contrast, the value of J became independent of k_* for the limit $k_* \to \infty$, which represents the case in which J is limited by the rate at which processes in the sediments occur. Based on the results shown in Fig. 10A, J is limited by turbulence in the water column if $k_* < 0.2$, whereas it is limited by sediment processes for $k_* > 3$. With respect to C_s (Fig. 10B), as k_* increases, the DO concentration at the WSI approaches C_W. On the contrary, for small values of k_*, the DO concentration at the WSI increases and reaches values up to several times C_W. However, to put this last result into perspective, recall that DO saturates in water, and
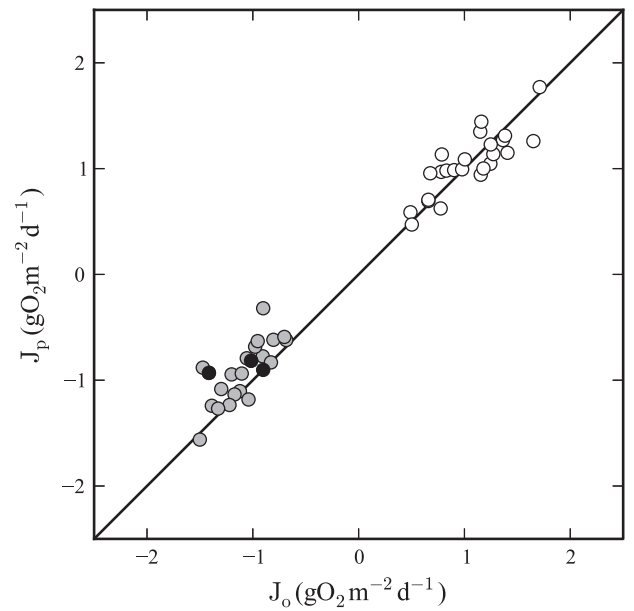

Fig. 9. Comparison of observed and predicted values of J calculated using Eq. (7) (white circles, $P_{ef} > 0$), Eq. (8) (gray circles where $P_{ef} < 0$ and DO is completely consumed within δ_p) and Eq. (9) (black circles).
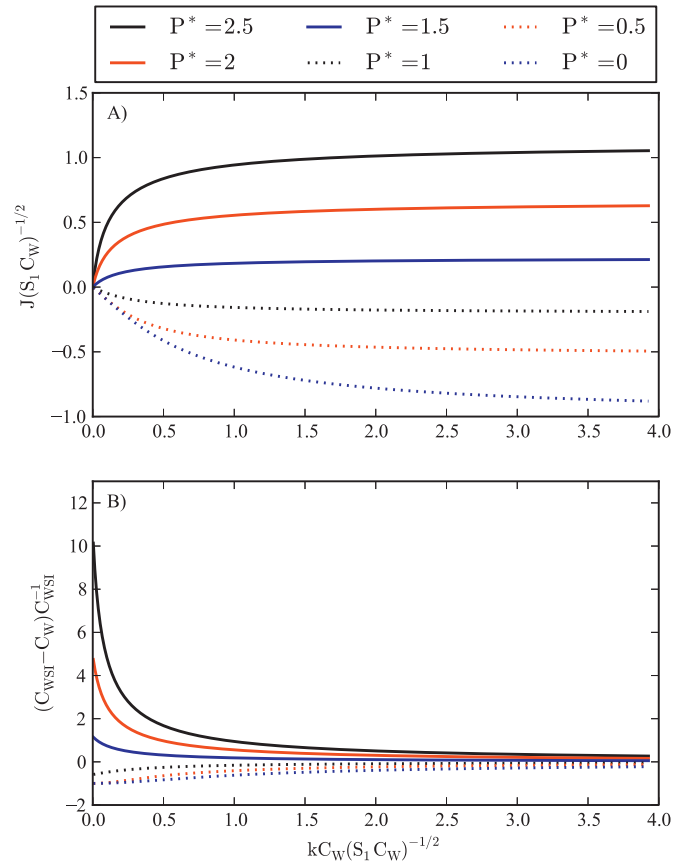

Fig. 10. The maximum DO flux consumed in homogeneous sediment as function of $k_* = kC_W(S_1 C_W)^{-1/2}$ for different DO production rates ($P_* = P(S_1 C_W)^{-1/2}$). (A) Flux of DO through the WSI calculated using Eqs. (7)–(9). (B) The difference between DO concentrations in the sediment and the water.
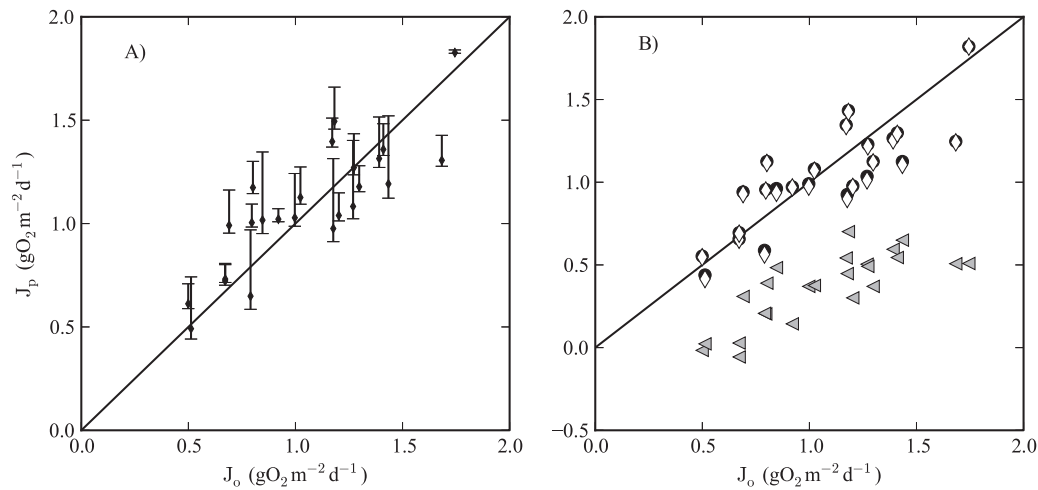
Fig. 11. (A) Sensitivity analysis of the calculated value of J as a function of α between 1 (lower limit of the error bars) and 2 (upper limit). (B) Sensitivity analysis to quantify the influence of using homogeneous rates of DO consumption assuming $\bar{r}_1 = \bar{r}_2$ (gray triangles) and $\bar{r}_2 = \bar{r}_1$ (white diamonds). Black circles were calculated with empirical data.

past the maximum concentration, oxygen bubbles start forming at the WSI.

3.5. Sensitivity analysis

An analysis was conducted to quantify how sensitive the estimation of J is to changes in α and to the use of two layers with different rates of DO consumption. Fig. 11A summarizes the results obtained by calculating J when $\alpha = 1$ (lower limit in vertical error bars) and when $\alpha = 2$ (upper limit in error bars). Black dots in Fig. 11A correspond to the values of J calculated using $\alpha = 1.21$, which was obtained from micro-profiles. As expected, the influence of $\alpha = 1$ on the calculated values of J was smaller than of $\alpha = 2$. This effect is because $\alpha = 1.21$ is closer to 1 than 2. Furthermore, the magnitude of the influence of α in the estimation of J (amplitude of the error bar) is smaller than 20%. For instance, for $J_o \approx 1.5 \, \mathrm{g\,O_2\,m^{-2}\,d^{-1}}$, the amplitude of the error bar was of $0.25 \, \mathrm{g\,O_2\,m^{-2}\,d^{-1}}$ that is equivalent to 16% of J_p; while for the smaller values of J_o ($J_o \approx 0.8 \, \mathrm{g\,O_2\,m^{-2}\,d^{-1}}$), was approximately 14%.

The influence of the rates of DO consumption on the estimation of J was quantified by calculating J in two scenarios shown in Fig. 11B, one where $\bar{r}_1 = \bar{r}_2$ (gray triangles) and the second with $\bar{r}_2 = \bar{r}_1$ (white diamonds), while holding the rest of the parameters such as P constant. Black circles indicate values of J predicted with the observed data. Smaller DO consumption rates are reflected in larger values of J, which is due to the effective production. However, by holding the effective production (P_{ef}) constant while changing $\bar{r}_2$, the predicted values of J did not change with respect to the original predictions (black circles). This result indicates that the effective production $P_{ef} = P - \bar{r}_1 \delta_p$ is the key parameter that defines the magnitude of J.

4. Discussion

We studied the behavior of a calculation method of the flux of DO across the WSI interface where benthic primary production occurs in a thin layer on the top of the sediment. Processes on both sides of the WSI were taken into consideration. On the water-side of the WSI, the rate of diffusion of mass across the diffusive boundary layer increases with turbulence in the water column. In contrast, on the sediment side of the WSI, biochemical consumption and the production of DO coupled with molecular diffusion explain J. Looking at the problem from this perspective allowed us to propose a conceptual scheme to calculate J as a function of processes occurring on both sides of the interface. Depending on the magnitude of k, in the context of the dynamics in the sediment, J can either be limited by the water or the sediment side of the WSI. Similar results were obtained by Nakamura and Stefan (1994) and Mackenthun and Stefan (1998) when there was no DO production. More recently, de la Fuente (2014) studied DO exchanges across the WSI with benthic primary production in the field, again obtaining similar results; however, de la Fuente (2014) did not evaluate the vertical variability of primary production or different rates of DO consumption.

Although the context of this research was extremely shallow salty lagoons of northern Chile, the results presented here can be extended to similar shallow ecosystems including coastal lagoons (del Castillo and Farfán, 1997; López-González et al., 1998), coral reefs (Jimenez et al., 2008, 2011, 2012), shallow lagoons (Timms, 2005; Herb and Stefan, 2005; Alsterberg et al., 2011) or shallow fjords (Attard et al., 2014).

The advantage of having a vertically integrated approach for estimating J (Eqs. (7)–(9)) is that it can be used to directly understand DO budgets in shallow lagoons without being having to solve diffusion-reaction equations in the sediments. One of the possible applications of Eqs. (7)–(9) is the determination of the thickness of the oxygenated layer of sediments below the photosynthetic active layer. The thickness of this layer is controlled by P_{ef}, which does not diffuse into the atmosphere, and $\bar{r}_2$; specifically, DO is completely consumed at the depth $(P_{ef} - J)\bar{r}_2^{-1}$ below δ_p. For our experiments, this oxygenated layer of sediments below δ_p was approximately 5 mm thick. Below this surface layer, permanent anoxic conditions are expected to occur; within this layer, DO fluctuates depending on the diurnal cycles of respiration/production. The thickness of this layer is generally unaffected by k_t or P_{ef} (Fig. 8).

Two months of growth time were required to achieve adequate microalgal biomass. The entire set of experiments was conducted during two weeks to ensure that the physiological conditions of the benthic microalgae community remained similar. Following the inoculation of the tank with water from the artificial lagoon near the University campus, the structure and composition of the benthic community changed rapidly. These changes modify P_{ef} through direct changes in P, r_1 and δ_p. The coefficient α can also be modified

by temporal changes in the mat composition; however, J is largely unaffected by this coefficient. Further studies are required to better characterize DO exchanges across the WSI as a function of the benthic microalgae composition (abundance and richness).

DO exchanges across the WSI are controlled by processes on both sides of the WSI. Eqs. (7) and (9) were obtained by adopting this perspective for solving J and were successfully validated in laboratory experiments.

Acknowledgments

Appendix A.

A.1. Derivation of Eq. (5).

To obtain Eq. (5) from Eq. (2) it is required to compute the second integral of the diffusive fluxes, that is

$$\int_{-\delta_p}^{0} \int_{z}^{0} \phi D_s \frac{\partial^2 C}{\partial z^2} dz' dz = \int_{-\delta_p}^{0} \int_{z}^{0} \left(r(z') - p(z') \right) dz' dz \tag{A1}$$

with ϕD_s uniform. Then, following the standard integration, the inner integral can be written as:

$$\int_{z}^{0} \phi D_s \frac{\partial^2 C}{\partial z^2} dz' = \phi D_s \left(\frac{\partial C}{\partial z} \bigg|_z - \frac{\partial C}{\partial z} \bigg|_0 \right) \tag{A2}$$

where $-\phi D_s (\partial C/\partial z)|_0 = J$. With this, the outer integral of Eq. (A1) is written as

$$\int_{-\delta_p}^{0} \phi D_s \left(\frac{\partial C}{\partial z} \bigg|_z - \frac{\partial C}{\partial z} \bigg|_0 \right) dz = \phi D_s \left(C_{\delta_p} - C_{SWI} - J\delta_p \right) \tag{A3}$$

The double integral of $p(z)$ in Eq. (A1) is written in terms of α (Eq. (4)), and by considering that $r(z)$ is uniform equal to $\bar{r}_1$, Eq. (A1) is finally written as Eq. (5)

$$\phi D_s \left(C_{\delta_p} - C_{SWI} - J\delta_p \right) = \frac{\alpha P \delta_p}{2} - \frac{\bar{r}_1 \delta_p^2}{2} \tag{A4}$$

A.2. Derivation of Eq. (7).

To Eq. (7), the DO concentration at the WSI is obtained from Eq. (6) as

$$C_{WSI} = \frac{(P-J)^2}{S_2} - \frac{P \left(P - P_{ef} \right)}{S_2} + \frac{\Delta \bar{r} \delta_p \left(2J - P_{ef} \right)}{S_2} - \frac{(1-\alpha) \bar{r}_2 \delta_p P}{S_2} \tag{A5}$$

With this, $J = -k \left(C_W - C_{WSI} \right)$ from the water-side of the WSI (Eq. (1)) can be written as

$$J = -\frac{k}{S_2} \left(S_2 C_W - (P-J)^2 + P \left(P - P_{ef} \right) \right.$$
$$\left. - \Delta \bar{r} \delta_p \left(2J - P_{ef} \right) + (1-\alpha) \bar{r}_2 \delta_p P \right) \tag{A6}$$

Finally, terms associated to J^2 and J are grouped to form the second order polynomial equation, whose negative root is Eq. (7). The positive root gives $J > P$ that has no real meaning.

References

Alsterberg, C., Hulth, S., Sundbacka, K., 2011. Response of a shallow-water sediment system to warming. Limnol. Oceanogr. 56, 2147–2160.

Arega, F., Lee, J., 2005. Diffusional mass transfer at sediment–water interface of cylindrical sediment oxygen demand chamber. J. Environ. Eng. 131 (5), 755–766.

Attard, K.M., Glud, R.N., McGinnis, D.F., Rysgaard, S., 2014. Seasonal rates of benthic primary production in a Greenland fjord measured by aquatic eddy correlation. Limnol. Oceanogr. 59, 1555–1569.

Boudreau, B.P., 1996. A method-of-lines code for carbon and nutrient diagenesis in aquatic sediments. Comput. Geosci. 22, 479–496.

Boudreau, B.P., Jørgensen, B.B., 2001. The Benthic Boundary Layer. Oxford University Press.

Bryant, L., McGinnis, D., Lorrai, C., Brand, A., Little, J., Wüest, A., 2010. Evaluating oxygen fluxes using microprofiles from both sides of the sediment–water interface. Limnol. Oceanogr. 8, 610–627.

Cerco, C., Seitzinger, S., 1997. Measured and modeled effects of benthic algae on eutrophication in Indian River-Rehoboth bay, Delaware. Estuaries 20, 231–248.

Dade, W.B., 1993. Near-bed turbulence and hydrodynamic control of diffusional mass transfer at the sea floor. Limnol. Oceanogr. 38, 52–69.

de la Fuente, A., 2014. Heat and dissolved oxygen exchanges between the sediment and water column in a shallow salty lagoon. J. Geophys. Res. Biogeosci. 119, 596–613, http://dx.doi.org/10.1002/2013JG002413

de la Fuente, A., Niño, Y., 2010. Temporal and spatial features in the thermo-hydrodynamics of a shallow salty lagoon in Northern Chile. Limnol. Oceanogr. 55, 279–288.

Dejoux, C., 1993. Benthic invertebrates of some saline lakes of the Sud Lipez region, Bolivia. Hydrobiologia 267, 257–267.

del Castillo, E., Farfán, C., 1997. Hydrobiology of a salt pan from the Peninsula of 430 Baja California, Mexico. Int. J. Salt Lakes Res. 6, 233–248.

Demergasso, C., Chong, G., Galleguillos, P., Escudero, L., Martínez-Alonso, M., Esteve, I., 2003. Microbial mats from the Llamará salt flat, northern Chile. Rev. Chil. Hist. Nat. 76, 485–499 (in Spanish).

Díaz-Palma, P., Stegen, S., Queirolo, F., Arias, D., Araya, S., 2012. Biochemical profile of halophilous microalgae strains from high-andean extreme ecosystems (NE-Chile) using methodological validation approaches. J. Biosci. Bioeng. 113 (6), 730–736.

Guatieri, C., Gualtieri, P.D., 2008. Gas-transfer at unsheared free-surface. In: Gualtieri, C., Mihailovic, D.T. (Eds.), Fluid Mechanics of Environmental Interfaces. Taylor & Francis, pp. 131–160.

Hancke, K., Sorell, B.K., Lund-Hansen, L.C., Larsen, M., Hancke, T., Glud, R.N., 2014. Effects of temperature and irradiance on a benthic microalgal community: a combined two-dimensional oxygen and fluorescence imaging approach. Limnol. Oceanogr. 59, 1599–1611.

Herb, W.R., Stefan, H.G., 2005. Dynamics of vertical mixing in a shallow lake with submersed macrophytes. Water Resour. Res. 41, W02023, http://dx.doi.org/10.1029/2003WR002613

Hulbert, S., Chang, C., 1983. Ornitholimnology: effects of grazing by the Andean Flamingo (Phoenicoparrus andinus). Proc. Natl. Acad. Sci. U.S.A. 80, 4766–4769.

Jimenez, I., Kühl, M., Larkum, A.W.D., Ralph, P.J., 2008. Heat budget and thermal microenvironment of shallow-water corals: do massive corals get warmer than branching corals? Limnol. Oceanogr. 53, 1548–1561.

Jimenez, I., Kühl, M., Larkum, A.W.D., Ralph, P.J., 2011. Effects of flow and colony morphology on the thermal boundary layer of corals. J. R. Soc. Interface 8, 1785–1795.

Jimenez, I., Larkum, A.W.D., Ralph, P.J., Kühl, M., 2012. In situ thermal dynamics of shallow water corals is affected by tidal patterns and irradiance. Mar. Biol. 157, 1773–1782.

Jørgensen, B.B., Boudreau, B.P., 2001. Diagenesis and sediment-water exchange. In: Boudreau, B.P., Jørgensen, B.B. (Eds.), The Benthic Boundary Layer. Oxford University Press, pp. 211–244.

Jørgensen, B.B., Des Marais, J., 1988. Optical properties of benthic photosynthetic communities: fiber-optic studies of cyanobacterial mats. Limol. Oceanorg. 33, 99–113.

Jørgensen, B.B., Des Marais, J., 1990. The diffusive boundary layer of sediments: oxygen microgradients over a microbial mat. Limnol. Oceanogr. 35, 1242–1255.

Jørgensen, B.B., Revsbech, N., Cohed, Y., 1983. Photosynthesis and structure of benthic microbial mats: microelectrode and SEM studies of four cyanobacterial communities. Limnol. Oceanogr. 28, 1075–1093.

Kampf, S., Tyler, S., Ortiz, C., Muñoz, J., Adkins, P., 2005. Evaporation and land surface energy budget at the Salar de Atacama, Northern Chile. J. Hydrol. 310, 236–252.

Kühl, M., Jørgensen, B.B., 1992. Microsensor measurements of sulfate reduction and sulfide oxydation in compact microbial communities of aerobic biofilms. Appl. Environ. Microbiol. 58, 1164–1174.

López-González, P.J., Guerrero, F., Castro, M.C., 1998. Seasonal fluctuation in the phytoplankton community in a hypersaline temporary lake (Honda, southern Spain). Int. J. Salt Lakes Res. 6, 353–371.

MacIntyre, H.L., Cullen, J.J., 1995. Fine-scale vertical resolution of chlorophyll and photosynthetic parameters in shallow-water benthos. Mar. Ecol. Prog. Ser. 122, 227–237.

MacIntyre, H.L., Geider, R.J., Miller, D.C., 1996. Microphytobenthos: the ecological role of the "secret garden" of unvegetated, shallow-water marine habitats. I. Distributio, abundance and primary production. Estuaries 19, 186–201.

Mackenthun, A., Stefan, H.G., 1998. Effect of flow velocity on sediment oxygen demand: experiments. J. Environ. Eng. 124, 222–230.

Mascitti, V., Kravetz, F., 2002. Bill morphology of the South American flamingos. Condor 104, 73–83.

Nakamura, Y., Stefan, H.G., 1994. Effect of flow velocity on sediment oxygen demand: theory. J. Environ. Eng. 120, 996–1016.

O'Connor, B., Hondzo, M., 2008. Dissolved oxygen transfer to sediment by sweep and eject motions in aquatic environments. Limnol. Oceanogr. 53, 566–578.

Rasmussen, H., Jørgensen, B.B., 1992. Microelectrode study of seasonal oxygen uptake in a coastal sediment: role of molecular diffusion. Mar. Ecol. Prog. Ser. 81, 289–303.

Revsbech, N., Jorgensen, B.B., Brix, O., 1981. Primary production of microalgae in sediments measured by oxygen microprofile, $H_{14}CO_3^-$ fixation, and oxygen exchange methods. Limnol. Oceanogr. 26, 717–730.

Revsbech, N., Madsen, B., Jørgensen, B.B., 1986. Oxygen production and consumption in sediments determined at high spatial resolution by computer simulation of oxygen microelectrode data. Limnol. Oceanogr. 31, 293–304.

Risacher, F., Alonso, H., Salazar, C., 2003. The origin of brines and salts in Chilean salars: a hydrochemical review. Earth Sci. Rev. 64, 249–293.

Sohma, A., Sekiguchi, Y., Kuwae, T., Nakamura, Y., 2008. A benthic–pelagic coupled ecosystem model to estimate the hypoxic estuary including tidal flat – model description and validation of seasonal/daily dynamics. Ecol. Mod. 215, 10–39.

Steinberger, N., Hondzo, M., 1999. Diffusional mass transfer at the sediment–water interface. J. Environ. Eng. 125, 192–200.

Timms, B., 2005. Salt lakes in Australia: present problems and prognosis for the future. Hydrobiologia 552, 1–15.

Wetzel, R., 2001. Limnology, 3rd edition. Academic Press.